Ultrafast Vibrational Dynamics of NO and CO Adsorbed on an Iridium Surface

Ian M. Lane,[†] Zhi-Pan Liu,[‡] David A. King,[†] and Heike Arnolds*,[§]

*Department of Chemistry, University of Cambridge, Lensfield Road, Cambridge CB2 1EW, United Kingdom,
Shanghai Key Laboratory of Molecular Catalysis and Innovative Materials, Department of Chemistry,
Fudan University, Shanghai, 200433, People's Republic of China, and Surface Science Research Centre,
The University of Liverpool, Oxford Street, Liverpool L69 3 BX, United Kingdom*

Hot electrons created by femtosecond laser pulses can transiently increase the occupation of the antibonding $2\pi*$ orbital of a diatomic adsorbate and change its bonding configuration. By monitoring the intramolecular stretch frequency of CO and NO on Ir{111} with time-resolved sum frequency spectroscopy, we demonstrate how the vibrational dynamics depend on the degree of charge flow between the surface and the adsorbate. We find CO and NO to be model adsorbates for adiabatic and nonadiabatic dynamics, respectively.

1. Introduction

Creation of electron−hole pairs is the only effective route of energy flow from high frequency internal adsorbate vibrational modes to metal surfaces. A dramatic example of this is the emission of hot electrons from a metal surface when highly vibrationally excited NO is scattered off it.[1] This questions the validity of the Born−Oppenheimer approximation of separable electronic and nuclear motion in surface chemistry, in particular, with regard to the nature of the transition state in a surface reaction.[2]

The importance of nonadiabatic dynamics has long been recognized in surface femtochemistry and was recently reviewed by Frischkorn and Wolf.[3] In particular, femtosecond infrared and infrared−visible sum frequency spectroscopies have been the leading tools in unravelling nonadiabatic vibrational dynamics, since an intense femtosecond pump pulse leaves electrons and phonons out of equilibrium for up to a few picoseconds. This allows one to distinguish experimentally between electron-driven and phonon-driven contributions to transient changes by measuring the coupling times with which the internal stretching mode of an adsorbate responds to an ultrafast heating pulse.[4−7]

The underlying physical picture of the observed dynamics is that of an indirect energy flow to electrons and phonons via low-frequency vibrational modes of the molecule: the internal A−B stretch frequency depends on the bonding position on the surface and thus couples anharmonically to a low-frequency mode, like the frustrated translation or rotation, which changes the bonding configuration.

The adsorbate's vibrational response to disturbing the equilibrium between electrons and phonons has been investigated exclusively for CO on a range of transition metal surfaces: platinum,[4,6] copper[8,9] and ruthenium.[5,7] Generally, for weak femtosecond excitation, coupling of the C−O stretch to the frustrated translation is found, while under desorption conditions coupling to the frustrated rotation has to be included.[5,6]

None of these studies have seen direct energy flow from the hot substrate electrons to the internal A−B vibration, despite the reverse process being the main energy relaxation channel for this mode.[10]

In this paper, we discuss the observation of direct energy flow from hot electrons to the internal molecular vibration on a subpicosecond time scale for NO on Ir{111}, which manifests itself in a red shift of the frequency and a strong increase in vibrational line width.[11]

The reason why no such effect has been observed for adsorbed CO lies in the height of the adsorbate $2\pi*$d orbital above the Fermi level and its resonant excitation through the hot electron Fermi distribution, as we will show here by comparing CO to NO on the close-packed iridium surface. NO on this surface has an antibonding orbital much closer to the Fermi level than CO, and hot electrons cause a change in the bonding configuration.

The detailed comparison of the ultrafast vibrational dynamics of these two adsorbates forms the core of the present paper. We show in this publication that our previously introduced model for coupling of hot electrons to the N−O stretch[11] correctly predicts the switch in nonadiabatic to adiabatic behavior as we change the adsorbate from NO to CO.

The paper is structured as follows: in section 2, we present the theoretical framework to explain the different behaviors of these two molecules; section 3 briefly outlines the experimental pump−probe method, while we analyze and discuss the experimental results in sections 4 and 5.

2. Theory

Before we go into details of our model, we will briefly describe what is known to happen to the adsorbate−substrate system after excitation by a femtosecond laser pulse with photon energy $h\nu$. An in-depth account can be found in ref 3.

Initially, the laser pulse creates a nonequilibrium electron distribution in the substrate with a maximum electron energy of $h\nu$. Electron−electron scattering then leads to a thermalized electron distribution within a few hundred femtoseconds, depending on the substrate and excitation density. Subsequently, the electrons equilibrate with the substrate phonons within a few picoseconds.

Electrons and phonons can subsequently couple with the adsorbate degrees of freedom. For energy transfer from the

---

* Corresponding author.
[†] University of Cambridge.
[‡] Fudan University.
[§] The University of Liverpool.

Ultrafast Vibrational Dynamics of NO and CO

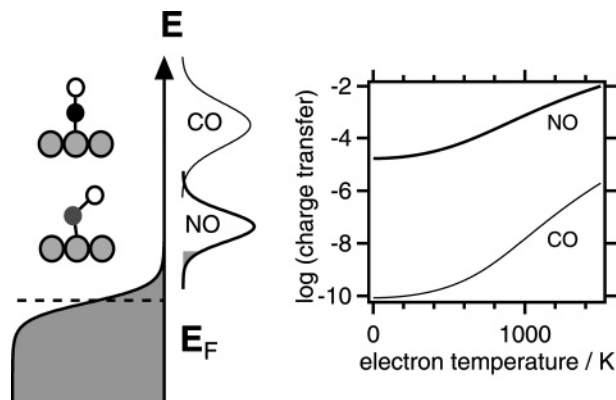*J. Phys. Chem. C, Vol. 111, No. 38, 2007* **14199**

Figure 1. Left: schematic diagram showing a thermalized hot Fermi-Dirac electron distribution and NO and CO antibonding $2\pi^*$ orbitals at 1.5 and 3.0 eV, respectively, and the effect on the adsorbate geometry. Right: dependence of charge-transfer magnitude on electron temperature for NO and CO.
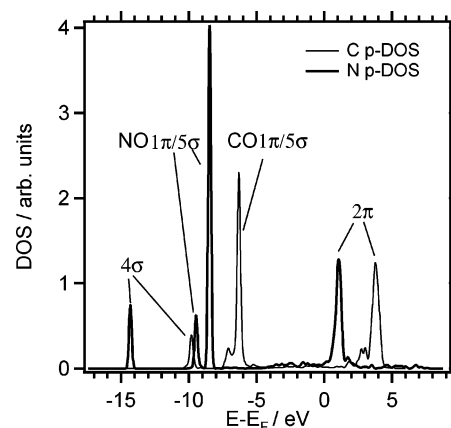

Figure 2. Density of states of the bare Ir{111} surface and saturated CO and NO layers on Ir{111}. Shown are the N 2p and C 2p contributions to the final wave function. The various peaks are labeled according to their molecular derived orbitals.

substrate electrons to the adsorbate, two different approaches have been used: electronic friction[12] and desorption induced by multiple electronic transitions (DIMET).[13]

The DIMET regime is typically observed for a width of the adsorbate level which is narrow relative to its energy measured from E_f. In the DIMET model, hot electrons transfer the adsorbate to an electronically excited potential energy surface with ensuing nuclear motion along the reaction coordinate before it relaxes back to a vibrationally excited level in the ground state. Multiple excitation/de-excitation cycles can enable the adsorbate to climb the vibrational ground state ladder to overcome the reaction barrier. This regime can also be described in form of a highly temperature-dependent electronic friction coefficient.

The electronic friction model is based on the Anderson–Newns model[14,15] of an adsorbate-derived affinity level, which shifts downward and broadens as the adsorbate approaches the surface. If this level is transiently populated by substrate electrons, then adsorbate motion away from the surface is induced. If the resonance width is large compared with kT and of the order of the distance of the resonance from the Fermi level, the resulting friction coefficient is largely temperature-independent.[12]

In terms of a DIMET versus electronic friction description, CO with its high lying $2\pi^*$ level (3–5 eV above E_f) is a representative of the DIMET mechanism, while NO with the $2\pi^*$ around 1.5 eV above E_f is expected to show a temperature-independent friction coefficient.

Electronic friction is related to the dominant vibrational relaxation mechanism for high frequency adsorbate vibrations: for adsorbed NO and CO, the $2\pi^*$ molecular orbital has broadened into a resonance which is partially occupied by metal electrons via back-donation. As the molecular bond length changes during the period of a vibration, the center of this resonance shifts up and down, leading to fluctuating charge transfer and therefore vibrational relaxation.

The following theoretical description of CO and NO pump–probe data is based on the idea of changing LUMO occupancy through a temperature-dependent charge transfer from the Fermi distribution of the metal electrons. This leads to a transient hybridization between Ir d_{z^2} and adsorbate $2\pi^*$ orbitals, which weakens the internal adsorbate bond and leads to a strong red shift of the frequency when hot electrons are present.

Figure 1 shows a schematic diagram of a hot Fermi-Dirac distribution n_f relative to an antibonding adsorbate orbital Π_{ads}.

The charge transfer integral depends strongly on the electron temperature and the position of the adsorbate level, as shown in Figure 1. It is clear that the charge transfer at a given electron temperature will be orders of magnitude larger for NO than for CO.

The nature of the antibonding orbital of these simple adsorbates is explained in a refined version of the Blyholder model of donation and back-donation.[16] For CO and NO on transition metals, the bonding is dominated by mixed adsorbate–metal states of 5σd and $2\pi^*$d character. As the metal d band levels shift up in energy from the right to the left of the periodic table, the overlap with the $2\pi^*$ orbital increases, thus, weakening the C–O or N–O bond at the same time as strengthening the adsorbate–metal bond.

Unlike CO, where the $2\pi^*$d orbital is around 3–5 eV above the Fermi level and relatively inaccessible to hot electrons, the NO $2\pi^*$ d is only 1.5 eV above E_f as measured by inverse photoemission on a number of transition metal surfaces.[17–19] No experimental values are presently available for the Ir{111} surface, and we have therefore used density functional theory (DFT) to calculate the density of states (DOS) for saturated CO and NO layers on Ir{111} as shown in Figure 2. The DFT calculation predicts the NO level at 1.0 eV and the CO level at 3.8 eV. These values should be regarded as lower limits for the lowest unoccupied molecular orbitals (LUMOs), as present density functionals tend to underestimate the cost of breaking a CO or NO bond. This has been accounted for by Kresse and co-workers,[20,21] who showed for example that the CO $2\pi^*$ orbital on Pt{111} should be 0.75 eV closer to the vacuum level than predicted by standard DFT. We would therefore expect experimental values for both $2\pi^*$d levels on iridium to be higher than shown in Figure 2.

A changing $2\pi^*$d occupation changes the internal bond strength, which in turn changes the stretching frequency. The quantitative relationship between the C–O frequency and the occupation of the $2\pi^*$d orbital has been calculated by Baerends and Ros for transition metal carbonyl complexes.[22] The relationship is linear with a gradient of -860 cm^{-1} per electron. A decrease in the N–O stretch frequency with increasing electron occupancy of the antibonding $2\pi^*$ orbital has been measured for a range of nitrosyl complexes by Fenske.[23] An additional electron reduces the frequency by 500 cm^{-1}. This decrease in frequency accompanies a change in bonding geometry. For nitrosyl complexes of the form $\{ML_5NO\}^n$, where n is the number of d electrons, the MNO group is linear when $n \leq 6$ and bent when $n \geq 7$.[24]
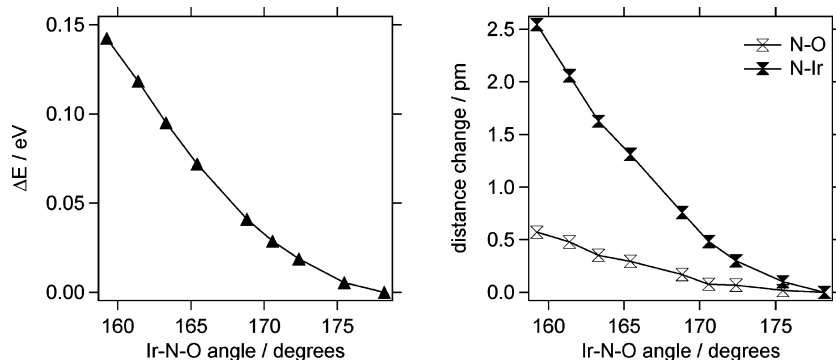
Figure 3. Energy change and N−O and N−Ir distances upon NO bending.

To calculate the effect a bending of the Ir−N−O group would have on the N−O stretch frequency, we have used DFT.[25] In the calculation, the *y* coordinate of the oxygen atom is fixed at various positions, while all other parameters are allowed to relax. The energy of this bent NO with respect to the relaxed state (NO upright) is calculated, as well as the optimized Ir−N−O angle and the frequency of the NO group. The results are shown in Figure 3.

We calculated the equilibrated adsorption state of atop NO in a p(2×2) layer at saturation coverage (0.5 monolayer, ML), where half the molecules reside in atop sites, the other half in fcc hollow sites. This atop NO has a bending angle of 178°, an N−O distance of 1.1758 Å, and a stretching frequency of 1915 cm^{-1}. At a bending angle of 162°, the N−O distance increases to 1.180 Å, the frequency drops by 54 cm^{-1} to 1861 cm^{-1}, and the total energy of the system has increased by $\Delta E = 0.12$ eV. As the molecule bends, the N atom shifts away from the atop position, so the N−Ir bond lengthens at the same time as the N−O bond, as shown in Figure 3. Bending therefore weakens both bonds.

In addition to the geometry, we have also calculated the electron gain of the NO 2π*d orbital with DFT, which for the largest angle (159°) is 0.03 e^{-}. This confirms our assumption from inorganic data that bent adsorbate geometry and increased 2π*d occupation are closely related for NO.

We recently incorporated this relationship between 2π*d occupancy, geometry of the Ir−N−O group, and N−O stretch frequency in a new model for time-resolved pump-SF probe spectroscopy,[11] which we will briefly review here.

We model the adsorbate frequency shift as a sum of two components: a thermal component ν_{lat}, which derives from electrons and lattice being in equilibrium, and an electronic component ν_{el}, which derives from the thermalized hot electrons.

$$\nu(t) = \nu_{lat}(t) + \nu_{el}(t) \tag{1}$$

We calculate the thermal component ν_{lat} on the basis of the statically measured linear temperature dependence with gradient ξ and frequency ω_0 at 100 K:

$$\nu_{lat}(t) = \omega_0 - (T_{lat}(t) - 100 \text{ K}) \cdot \xi \tag{2}$$

The electronic contribution is driven by the magnitude of charge transfer between the Fermi distribution and the adsorbate orbital. This magnitude $A(T_{el})$ increases with electron temperature as shown in Figure 1, and the adsorbate frequency responds to this within a time τ_{el}. The faster the response time, the higher is the degree of nonadiabaticity. τ_{el} can be thought of as the time it takes the nuclei to move in response to a change in 2π*d occupation.

$$\frac{d\nu_{el}(t)}{dt} = -A(T_{el}) + \frac{1}{\tau_{el}} \cdot \nu_{el}(t) \tag{3}$$

$$A(T_{el}) = \beta \cdot \int_{-\infty}^{\infty} n_f(\epsilon) \, \Pi_{ads}(\epsilon) \, d\epsilon \tag{4}$$

where $\epsilon = E - E_f$ is the energy with respect to the Fermi energy E_f and the adsorbate orbital is taken as a Gaussian centered at ϵ_a with width Γ. The degree of overlap is converted into a frequency shift with a numerical factor β.[11]

Together with the frequency changes, we need to model the instantaneous line width changes. We again use a sum of a thermal component Γ_{lat} (the extrapolated static temperature dependence of the line width) and an electronic component Γ_{el}. For the latter, we use an empirical model of coupling the instantaneous line width change to the difference between electron and lattice temperature $T_{el} - T_{lat}$ with the above time constant τ_{el} and a linear gradient.

$$\frac{d\Gamma_{el}(t)}{dt} = \alpha(T_{el} - T_{lat}) + \frac{1}{\tau_{el}} \cdot \Gamma_{el}(t) \tag{5}$$

NO shows large transient changes in line width, and it is essential that we model these changes correctly, as the time resolution of the SF probe is mainly determined by the overall vibrational relaxation time T_2 of the observed mode. At 100 K, this relaxation time is 1.5 ps for NO and 1.9 ps for CO.[26] An increased transient line width therefore means increased time resolution.

In the final step of modeling, instantaneous frequency and width changes are used as an input to the optical Bloch equations for direct comparison with pump−probe data.[7]

3. Experimental Section

A full description of the femtosecond sum frequency setup can be found elsewhere.[27,28] Briefly, a Spectra Physics 10 Hz regeneratively amplified Ti:S system delivers 140 fs pulses at 7 mJ of energy per pulse. A LightConversion optical parametric amplifier (TOPAS) with noncollinear difference frequency stage is pumped by 2.5 mJ of this to produce mid-infrared pulses. 2 mJ are passed through a pulse-shaper to produce narrow-band visible pulses used for sum frequency generation (SFG) up-conversion. The rest of the beam (2.5 mJ) is used to provide pump pulses at 800 nm with variable energy and polarization. For pump pulses of lower photon energy, this beam is used to pump a second TOPAS and either the idler or the signal wavelengths are then used for pumping. The IR beam enters the chamber at 65° to the surface normal; the 800 nm upconversion beam and the pump beam enter at 60°. All beams
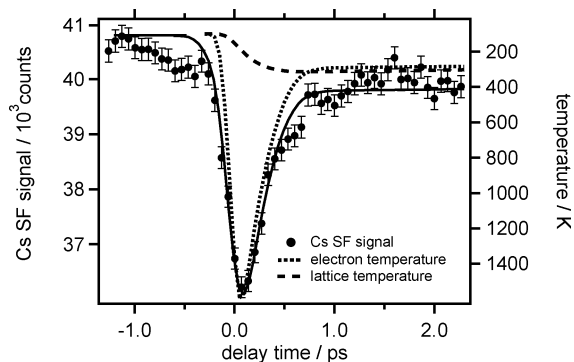
Ultrafast Vibrational Dynamics of NO and CO

J. Phys. Chem. C, Vol. 111, No. 38, 2007 **14201**

Figure 4. Nonresonant Cs sum frequency signal as a function of time delay between a 20 Jm^{-2} 800 nm pump pulse and femtosecond SF probe pulses. The solid line is the scaled convolution of the electron temperature (dotted line) with a 200 fs probe pulse. Also shown is the calculated lattice temperature (dashed line).

pass through a 25 cm focal length CaF$_2$ lens. Because of the chromatic aberration of the lens, the pump beam spot is about three times larger than the IR beam spot, while the size of the upconversion beam has been matched to the size of the IR beam through a telescope arrangement.

Temporal and spatial overlap of all beams (pump, IR, and 800 nm upconversion) are optimized and checked on a temporarily deposited cesium multilayer on the iridium surface, and all beams are fully characterized by frequency resolved optical gating (FROG) and XFROG.[27] We find that pump pulses of around 25 J/m^2 reduce the Cs sum frequency signal by approximately 10% after optimization. Figure 4 shows the cesium signal as a function of time delay between an 800 nm pump and femtosecond SF probe pulses, together with a calculation of the time-dependent electron and lattice temperatures according to the two-temperature model (see Appendix for parameters). The reduction in Cs signal nicely follows the calculated electron temperature convoluted by the 200 fs width of the IR probe pulse. After alignment of the femtosecond beams, a slit is inserted in the pulse shaper to produce narrow band upconversion pulses, and the Cs signal minimization is checked for spatial optimum. All beams are p polarized unless otherwise noted.

NO adsorption on Ir{111} has been studied by electron energy loss spectroscopy (EELS)[29,30] and X-ray photoelectron spectroscopy (XPS).[31] At coverages less than 0.15 ML, NO occupies atop sites only at a frequency of 1860 cm^{-1} and dissociates completely upon heating. At the saturation coverage of 0.5 ML,[32] additional molecules reside in bridge or hollow sites with two characteristic frequencies around 1440 and 1550 cm^{-1}. On heating a saturated layer, the molecules from low-frequency sites desorb first, and the atop molecules desorb as well as dissociate. We only observe NO in atop sites in SFG; the lower frequency species are too weak to be detected.

CO adsorption on Ir{111} has been investigated by SFG, RAIRS, and LEED.[33−35] Only atop sites are occupied, with a $(\sqrt{3}\times\sqrt{3})R30°$ structure formed at 0.33 ML and a $(2\sqrt{3}\times2\sqrt{3})R30°$ structure formed at 0.58 ML. CO in the latter structure has an internal frequency of 2080 cm^{-1}.

Pump−probe transients, typically take between 30 min and 2 h to record, depending on signal levels. Long-term stability of the adlayer coverage and shot-to-shot reproducibility are therefore of vital importance. The majority of results presented here were conducted on saturated NO (0.5 ML) and CO (0.58 ML) layers. For fluences high enough to cause desorption, this ensures that the adlayer can be simply redosed between shots

from the gas phase at background pressures up to 10^{-6} mbar. In addition, NO in hollow sites prevents ultimate dissociation of the atop NO by site-blocking.

4. Results

4.1. Static Temperature Dependence. The measured static temperature dependence is the necessary input for modeling the thermal component of the pump-induced changes.

The change in frequency and width of the CO and NO sum frequency peaks is shown in Figure 5. The CO data were acquired at fixed temperatures during heating, while the NO data were recorded during an 8 K/min ramp of the sample to 290 K and cooling back to 100 K. The frequency shows a strong red shift of −5 and −10 cm^{-1} for CO and NO respectively from 100 to 290 K, while the line width increases for both molecules by 4 cm^{-1}. Both changes are reversible upon cooling.

The red shift can be explained by coupling of the intramolecular stretching mode to the frustrated translation or rotation.[36] The frequencies of these modes for CO and NO on iridium are not known, but they are mainly dependent on the bonding site and less dependent on the transition metal. For example, on Rh{111}, on-top bonded NO in a p(2×2) layer has a frustrated translational frequency of 59 cm^{-1}, while CO has a frequency of 44 cm^{-1} in the $(\sqrt{3}\times\sqrt{3})R30°$ structure.[37] Frustrated rotations typically have frequencies in the 400−500 cm^{-1} range.

4.2. Time-Resolved Spectroscopy. *4.2.1. Shape of the Transients.* Figure 6 shows the changes to the CO and NO stretch frequencies and line widths at 100 K base temperature as a function of pump−probe delay time for an 800 nm pump pulse. The shapes of the transients are dramatically different. While the CO spectra only show a gradual return to the unpumped value on a time scale of 100 ps,[38] the NO spectra show an additional fast change within ±2 ps of zero time delay. The two time scales in the NO transient are reminiscent of the evolution of electron and lattice temperatures after femtosecond laser heating (see Figure 4).

The CO transient can be fitted by just using the thermal component in eq 1, while the NO transient is well-described by thermal electron excitation into an orbital at 1.5 eV with a full width at half maximum (fwhm) of 0.7 eV and a coupling time of 700 fs. The existence of a fast electronic contribution to the NO spectra can be most clearly seen in the spectral shape at negative time delays. A fast change in the frequency causes a strongly perturbed free induction decay and modulation of the spectra occurs at a frequency inversely proportional to the pump−probe delay ($\Delta\omega = 2\pi/\Delta t$).[28] Figure 7 shows NO spectra together with two sets of calculated spectra scaled by the same factor for all delay times.[39] For one set, we used the model parameters given above, and for the other set, we used a much faster frequency change directly proportional to the electron temperature. It can be clearly seen that our model (where the frequency changes on the 700 fs time scale) fits the shape and magnitude of the oscillations very well, while a direct input from T_{el} (where the frequency changes on a 100 fs time scale) would distort the spectra too much.

This lack of very fast change strongly indicates that we have no direct electron excitation into an unoccupied adsorbate orbital.

4.2.2. Pump Wavelength and Polarization Dependence. In order to prove our model assumption that thermalized electrons, not nascent hot electrons, are responsible for the observed NO transient, we varied the photon energy of the pump beam, using photon energies of 3.10 eV (400 nm, p polarized) and 0.77 and 0.89 eV (1590 and 1396 nm, s polarized). These wavelengths
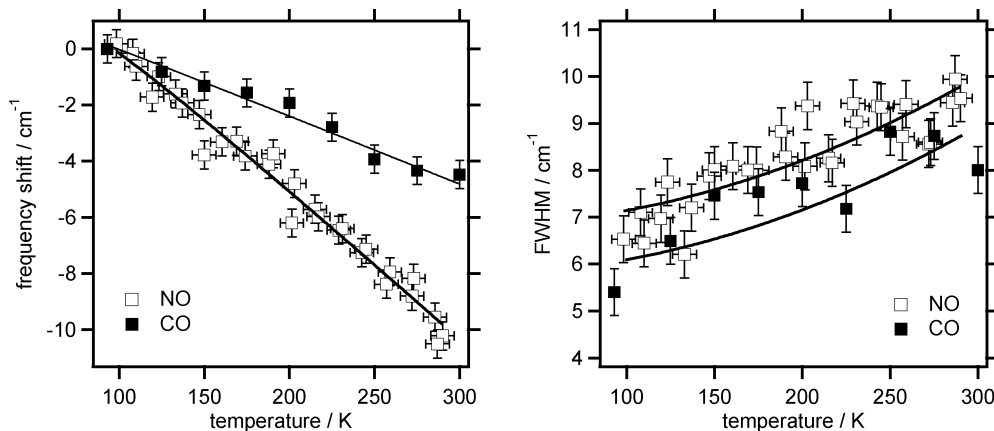
Figure 5. Static temperature dependence of the frequency and line width of CO and NO. Solid lines in the frequency graph are linear fits; solid lines in the line width graph are guides to the eye.
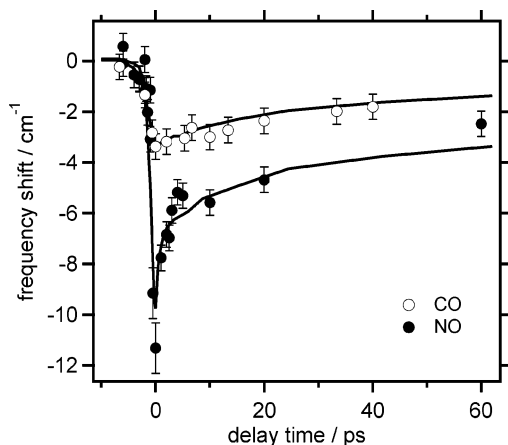

Figure 6. Time dependent changes in the frequency of SFG peaks of 0.43 ML CO and 0.5 ML NO adsorbed on Ir{111} at 100 K after pumping with a 150 fs 800 nm pulse at an adsorbed fluence of 12 respectively 10 Jm^{-2}.

were generated by various nonlinear processes with different beam size, divergence and absorbance, but we could find no quantitative difference to the 1.55 eV pump data within the uncertainty of the pump fluence. Data points for 1396 nm pump are included in the fluence dependence shown in Figure 9. We also verified that the effects of the 800 nm pump pulse only depend on its absorbed intensity, not on its polarization.

This lack of wavelength and polarization dependence, together with an adsorbate response that is slower than the change in substrate electron temperature also exclude multiphoton absorption by the adsorbate as a possible cause of the NO transients.[40]

4.2.3. Fluence Dependence. The overlap of the hot electron distribution with the adsorbate orbital depends very strongly on temperature as shown in Figure 1. This manifests itself in a strong fluence dependence of the magnitude of the fast component in the NO transients. Figure 8 shows that at low fluences, NO follows the phonon temperature, while at higher fluences, perturbation of NO by the metal electrons is extremely pronounced. Such a pronounced fluence dependent change is unknown for adsorbed CO.[5,41] The solid lines in Figure 8 were calculated using the above model parameters of an 0.7 eV wide orbital centered at 1.5 eV with a coupling time of 700 fs and give an excellent description of the transients. The highest laser fluence of 15 J/m^2 shown in Figure 8 caused appreciable desorption within 1000 laser shots (approximately 10^{-4} ML/ shot).

The pump–probe data in Figures 6 and 8 show an evolution on two distinct time scales, which we name electronic and

thermal. A time delay of 0 ps was used to probe the electronic component, as this is near the maximum temperature difference between electrons and lattice. A value of +15 ps was chosen for the thermal component, long after electrons and phonons have equilibrated. The corresponding changes in frequency and line width, as a function of pump fluence, are shown in Figures 9 and 10 for NO and CO respectively. The importance of the electronic component in the NO data is obvious from the nonlinear frequency change with fluence; CO, in comparison, shows a linear fluence dependence both at 0 and at 15 ps.

Both the time-dependent and the fluence-dependent data confirm that adsorbed NO couples strongly to the electron bath, while CO does not. The data can be modeled very well with our electronic friction model. For CO, an electronic component is not necessary. For an orbital around 3 eV above E_f with 1 eV width, we would expect the electronic component at $t = 0$ ps to be far less than 1 cm^{-1} for the highest fluence used in Figure 10 and therefore negligible.

4.2.4. Probe Polarization Dependence. The transient occupation of the $2\pi^*$ NO orbital means hybridization with the metal d$_{z^2}$ orbital, causing bending of the adsorbate. SFG should be able to detect such bent NO, by changing the polarization of the visible upconversion beam and of the detected signal. In PPP geometry (all beams p polarized), the χ_{zzz} and χ_{xxz} elements of the nonlinear susceptibility tensor contribute to the measured signal; in SSP geometry (signal and visible beams s polarized), only χ_{yyz} contributes. The ratio of the two signals depends on the orientation of the adsorbate and its molecular hyperpolarizability ratio β_{aac}/β_{ccc} for $C_{\infty v}$ molecules like NO, where c denotes the molecular axis and a is an axis perpendicular to c. Our SFG intensity ratio I_{SSP}/I_{PPP} is approximately 0.03, independent of the surface temperature between 100 to 300 K. Following the discussion in ref 42, the bending angle can only be correctly deduced if the optical properties of the NO layer and the values of β_{aac}/β_{ccc} for adsorbed NO are known. However, to simply confirm the existence of a bent transition state, I_{SSP}/I_{PPP} can be followed as a function of pump–probe delay time.

When this experiment is carried out, the ratio decreases around time zero, which in a simplistic view might indicate a more upright NO. However, a meaningful evaluation of the data is hampered by two facts. Firstly, the reflectivity R of the interface can change by a few percent as a result of the pump beam,[43] which in turn modifies I_{SSP}/I_{PPP}, and we currently have no pump–probe reflectivity data to quantify this effect. Secondly, the hyperpolarizability ratio β_{aac}/β_{ccc} is bound to increase if the $2\pi^*$ occupation increases,[44] because electron density outside the

Ultrafast Vibrational Dynamics of NO and CO

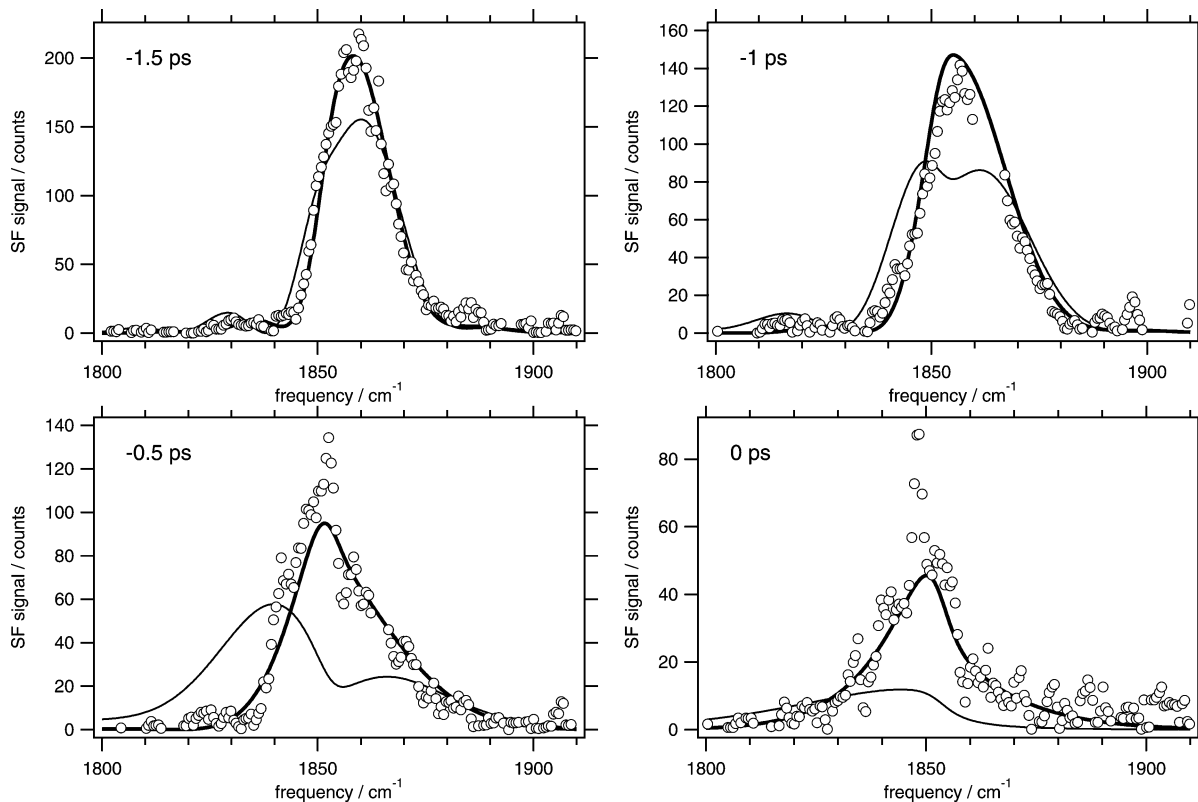*J. Phys. Chem. C, Vol. 111, No. 38, 2007* **14203**

Figure 7. Distortion of the spectral shape of the NO resonance through perturbation of free induction decay at negative time delays. Thin curves assume a very fast frequency change based on the surface electron temperature. Thick curves, slower frequency change according to the model.
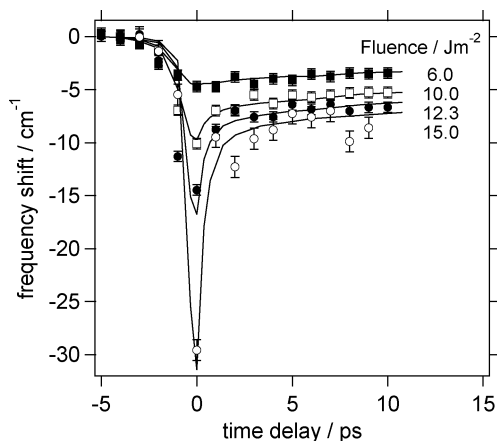

Figure 8. Fluence dependent transients for fluences of 6.0, 10.0, 12.3, and 15.0 Jm^{-2}. The highest fluence caused appreciable desorption within 1000 laser shots but constant coverage could be maintained with a background pressure of 2.5×10^{-7} mbar.

bond axis leads to a more spherical polarizability. Without additional time-resolved techniques, the concurrent changes in reflectivity, NO angle, and β_{aac}/β_{ccc} cannot be separated.

5. Discussion

Our experimental results can be briefly summarized as follows: as a result of ultrafast heating we find a transient N−O frequency, which changes on two time scales: a fast electronic one and a slow thermal one. Under similar excitation conditions, the C−O frequency shows only a thermal response (Figure 6). In addition, we find that the electronic contribution to the N−O frequency shift depends nonlinearly on fluence (Figure 8). We have modeled the pump−probe spectra under the following assumptions: the slow thermal response of both adsorbates is

caused by coupling to the same low-frequency mode that is responsible for the static temperature dependence shown in Figure 5. In addition, N−O spectra have an electronic component caused by charge transfer from hot electrons to the NO $2\pi^*$d orbital, which leads to internal bond weakening and bending of the adsorbate. The nuclear motion follows the electron excitation at a time scale of 700 fs. The electronic effect cannot be seen for CO, because the CO $2\pi^*$d orbital is too far above the Fermi level to be efficiently populated by hot electrons at transient temperatures below 2000 K.

Before we discuss the implications of our model, we will first address the question whether the results could have been modeled by indirect coupling to electrons via a low-frequency frustrated vibration.

We have attempted to describe our NO results within the well-known framework of an adsorbate heat bath, which couples to electrons and phonons with coupling times τ_{el} and τ_{lat}.[4] Regardless of whether we assume the frustrated translation or rotation as the coupling mode, it is impossible to fit all of the transients consistently with a constant τ_{el}. We would have to assume that an increasing electron temperature causes faster coupling between the low-frequency mode and the hot electrons by at least a factor 10, as we move from the lowest to the highest fluence.

Such a strongly temperature-dependent electron coupling time would be expected in the DIMET model for an adsorbate with a relatively narrow LUMO high above E_f, which is the case for CO and not for NO. But even for CO, expected temperature dependencies are more moderate. While a pump−probe study of the vibrational excitation of CO on Cu{100}[41] assumed a strong temperature dependence of τ_{el}, the measured changes were later re-interpreted to be the result of the anharmonic CO−substrate interaction potential,[45] based on temperature-dependent electron and phonon-induced lifetimes of the four vibrational
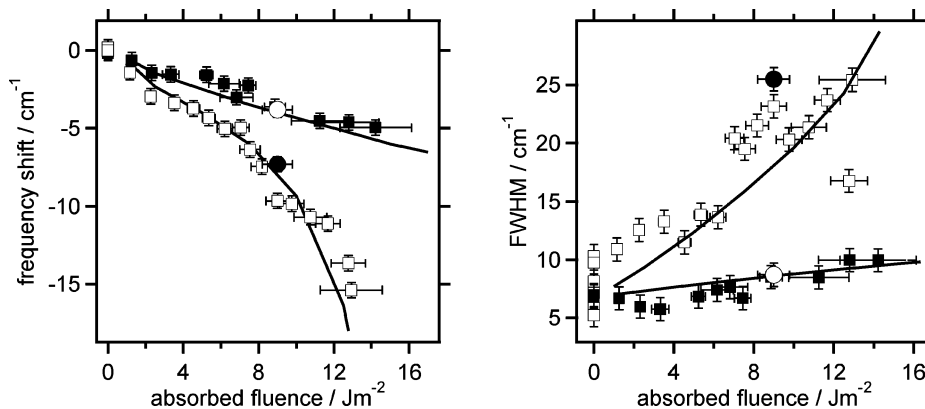
Figure 9. Fluence dependence of frequency shift and line width at $t = 0$ ps (electronic, open symbols) and $t = 15$ ps (thermal, closed symbols) for NO. Solid lines are fits to the data; see discussion for details. Large inverted symbols are data recorded at 9 Jm^{-2} with an 1396 nm pump beam.
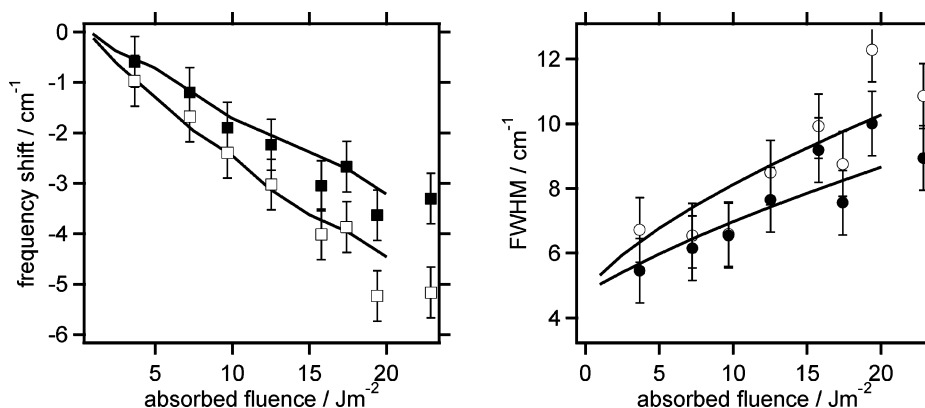

Figure 10. Fluence dependence of frequency shift and line width at $t = 0$ ps (electronic, open symbols) and $t = 15$ ps (thermal, closed symbols) for CO. Solid lines are fits to the data; see discussion for details.

modes calculated for CO on Cu{100}.[46] The strongest temperature dependence was found for the CO−surface stretch, with a lifetime that reduces by a factor of two when the temperature is increased from 10 to 450 K. Equally, changing the distance to the surface and the adsorbate orientation angle over a wide range changes the electronic friction coefficient by at most a factor four.[10]

While NO/Ir{111} will certainly be described by a different interaction potential than CO/Cu{100}, it seems unlikely to be anharmonic enough to justify such large changes in the electron coupling time. In fact, the main effect of a faster coupling time on the pump−probe transients is to increase the magnitude of the frequency shift. The maximum is also shifted to earlier times, but this is only a small effect due to the convolution with the adsorbate polarization decay time of around 1.5 ps. A stronger dependence on fluence is produced by assuming the higher frequency frustrated rotation as a coupling mode, but a reasonable fit to high fluence transients overestimates the fast component of low fluence data.

Considering that our main pump photon energy of 1.55 eV is near-resonant with the NO 2π*d orbital, we also have to address the question why we do not see an influence of nascent electrons. The electron−electron scattering time has been measured on the close-packed ruthenium surface[47] and is found to decrease strongly with increasing fluence. At the typical fluence of 16 Jm^{-2} in our experiments, we would expect the nascent electrons to equilibrate within 100 fs. But NO only reacts at a much slower time scale of 700 fs, and hot electrons will therefore dominate the transients. To produce CO transients similar in shape to NO, a low fluence near-resonant excitation of the CO 2π*d orbital would be needed.

Our new model explains the strong coupling between NO and electrons (and the lack thereof for CO) by transient occupation of the 2π*d orbital, which changes the adsorbate geometry from upright to bent because the adsorbate 2π* orbital hybridizes with the metal d_{z^2} orbital. From comparison with DFT calculations, we can deduce that the bending angle is around 15° just below the desorption threshold. This geometrical change is similar to the frustrated rotational mode, in that DFT predicts the nitrogen and oxygen will move in opposite directions. But the motion in our case is caused by a change in the bonding orbitals, not by frustrated rotational movement.

Bending of NO and CO is a prerequisite for dissociation, such that charge can flow into the 2π*d orbital and weaken the internal adsorbate bond. For example, flat lying or severely bent precursors to dissociation have been detected on Rh {100} and Ni{100}[48,49] for NO and on Cr{110} and Fe{100}[50,51] for CO. Similarly, C−O bond activation in the decomposition of methanol could be related to a change in the geometrical structure of the adsorption complex.[52] The key factor in the propensity of CO and NO to dissociate is the position of the metal d band with respect to the adsorbate 2π* orbital. An increased overlap has been found to strengthen the adsorbate metal bond and to weaken the internal adsorbate bond.[53] When the overlap is increased by femtosecond excitation, both bonds are weakened by a total of 0.14 eV at 20° bending angle. This corresponds to a tenth of the barrier to dissociation, but merely 0.03 e$^-$ additional charge is needed to accomplish this.

Our results therefore show that only relatively small amounts of charge are needed to considerably weaken the N−O bond and facilitate dissociation. Iridium might therefore be an ideal surface to control NO dissociation through alloying.

Ultrafast Vibrational Dynamics of NO and CO

J. Phys. Chem. C, Vol. 111, No. 38, 2007 **14205**

TABLE 1: Parameters Used for Calculating Laser Heating of Ir{111}

coefficient of electron specific heat[61]	γ	0.0031	J K^{-2} mol^{-1}
lattice heat capacity	C_{ph}	0.131	J g^{-1} K^{-1}
Debye temperature	Θ_D	430	K
second moment of phonon distribution[62]	$\langle \omega^2 \rangle$	342.83	meV^2
superconductivity e-ph coupling constant[63]	λ	0.45	
electron−phonon coupling constant	g	94.3×10^{16}	W m^{-3} K^{-1}
reflectivity at 800 nm and 62° incidence angle	R	0.51	
optical skin depth at 800 nm	δ	24.4	nm

Different behavior between NO and CO has been noted in photodesorption experiments from Pt{111} before, which show that NO leaves the surface with a higher rotational excitation than CO.[54] The rational for this was that an extra electron in the 2π* d orbital makes NO isoelectronic with O$_2$, which adsorbs with its molecular axis parallel to the platinum surface. Our results, together with quantum theoretical simulation of laser photodesorption by Saalfrank,[55] indicate that only a partial negative charge is needed, in a modification of the Antoniewicz negative ion resonance model.[56]

Finally, we address the observed line width changes. Both the CO and the observed NO are adsorbed in atop positions and show very similar increases in line width with substrate temperature (Figure 5). However, during pump−probe spectroscopy, the NO line width shows a much stronger increase with pump fluence than the CO line width (Figures 9 and 10). Under steady-state conditions it is known that the 2π* d orbital of CO and NO broadens into a resonance, which is partially occupied by metal electrons (back-donation). As the molecular bond length changes during the vibration, the center of this resonance shifts up and down, leading to fluctuating charge transfer (electronic friction) and therefore vibrational relaxation.[57]

The model presented here should be extended toward a quantitative theory for the connection between line width and electronic friction, as the observed increase contains valuable information on the bonding of the adsorbate. The increase can be rationalized, if not quantified, within the electronic friction model and consists of a lifetime and a dephasing contribution.

The short vibrational lifetime of the molecular stretch can be explained by charge transfer during one oscillation of the molecular bond, which shifts the adsorbate level with respect to E_f. In the limit of 0 K, the relationship between the inverse lifetime Γ and the amount of charge δn transferred during one oscillation of the N−O bond at frequency ω is given as:[58]

$$\Gamma(t) = \frac{2}{3} \pi \omega (\delta n)^2 \qquad (6)$$

This charge transfer will increase as the center-of-mass of the adsorbate moves closer to the metal surface, which is exactly what we expect to happen as the molecule bends.

There will also be a dephasing contribution to the line width, which is connected to the change in adsorbate geometry. Generally, multiply coordinated adsorbates have larger line widths, which also increase more strongly with temperature compared with singly coordinated ones.[36] This is due to a larger involvement of the 2π* orbital in bonding, resulting in a stronger interaction between the internal adsorbate stretch and the low-frequency frustrated vibrations. The line width increase in NO therefore also contains a contribution of dephasing induced by hot electrons via the bending motion and a concomitant change in 2π* bonding. It would therefore be valuable in the future to probe the pump-induced changes with IR pump−probe spectroscopy to separate lifetime from dephasing contributions.[26]

6. Conclusions

We have presented the first systematic comparison of the ultrafast dynamics of two catalytically important adsorbates, nitric oxide and carbon monoxide. We have shown that a model of transient charge transfer to an antibonding adsorbate orbital, which causes a geometric change in the adsorbate, can explain pump−probe transients for both CO and NO on Ir{111}. In particular, we find that NO bends in response to the hot electrons at a time scale of 700 fs. We have related the time-resolved results to the surface's propensity for dissociation of the adsorbate, since the deciding factor is the overlap between the metal d electrons and the antibonding orbital. The overlap is small for CO, which follows the pump-induced changes adiabatically. The improved overlap for NO induces nonadiabatic behavior, allowing us to observe direct energy flow from hot electrons to the internal adsorbate vibration in the time domain.

Appendix

The modeling of the laser-induced surface heating is based upon the two temperature model, which is used extensively in the literature and was initially proposed by Anisimov et al.[59] This involves numerically solving the following coupled differential equations:

$$C_e \frac{\partial T_e}{\partial t} = \kappa \nabla^2 T_e + g(T_{ph} - T_e) + S(z, t) \qquad (7)$$

$$C_{ph} \frac{\partial T_{ph}}{\partial t} = -g(T_l - T_e) \qquad (8)$$

where T_e and T_{ph} are the electron and lattice temperatures, κ is the thermal conductivity, C_{ph} is the lattice heat capacity, and $C_e = \gamma T_e$ is the electronic heat capacity where γ is the coefficient of the electronic specific heat and g is the electron−lattice coupling constant. The coupling constant can be derived as follows:[60]

$$g = -\frac{3\hbar\gamma}{\pi k_b} \lambda \langle \omega^2 \rangle \qquad (9)$$

where λ is the electron−phonon coupling constant used in superconductivity theory and $\langle \omega^2 \rangle$ the second moment of the phonon spectrum. Our calculated value agrees very well in the Cs pump−probe measurements. A summary of the parameters used to calculate the optical heating of iridium are given in Table 1.

References and Notes

(1) White, J. D.; Chen, J.; Matsiev, D.; Auerbach, D. J.; Wodtke, A. M. *Nature* **2005**, *433* (7025), 503−505.

(2) Wodtke, A. M.; Tully, J. C.; Auerbach, D. J. *Int. Rev. Phys. Chem.* **2004**, *23* (4), 513−539.

(3) Frischkorn, C.; Wolf, M. *Chem. Rev. 106* (10), 4207−4233.

(4) Germer, T. A.; Stephenson, J. C.; Heilweil, E. J.; Cavanagh, R. R. *J. Chem. Phys.* **1993**, *98* (12), 9986−9994.

(5) Bonn, M.; Hess, C.; Funk, S.; Miners, J. H.; Persson, B. N. J.; Wolf, M.; Ertl, G. *Phys. Rev. Lett.* **2000**, *84* (20), 4653−4656.

(6) Fournier, F.; Zheng, W. Q.; Carrez, S.; Dubost, H.; Bourguignon, B. *J. Chem. Phys.* **2004**, *121* (10), 4839−4847.

(7) Symonds, J. P. R.; Arnolds, H.; King, D. A. *J. Phys. Chem. B* **2004**, *108* (38), 14311−14315.

(8) Germer, T. A.; Stephenson, J. C.; Heilweil, E. J.; Cavanagh, R. R. *Phys. Rev. Lett.* **1993**, *71* (20), 3327−3330.

(9) Culver, J. P.; Li, M.; Jahn, L. G.; Hochstrasser, R. M.; Yodh, A. G. *Chem. Phys. Lett.* **1993**, *214* (5), 431−437.

(10) Tully, J. C. *Annu. Rev. Phys. Chem.* **2000**, *51*, 153−178.

(11) Lane, I.; King, D.; Liu, Z.; Arnolds, H. *Phys. Rev. Lett.* **2006**, *97*, 186105.

(12) Brandbyge, M.; Hedegard, P.; Heinz, T. F.; Misewich, J. A.; Newns, D. M. *Phys. Rev. B* **1995**, *52* (8), 6042−6056.

(13) Misewich, J. A.; Heinz, T. F.; Newns, D. M. *Phys. Rev. Lett.* **1992**, *68* (25), 3737−3740.

(14) Anderson, P. W. *Phys. Rev.* **1961**, *124* (1), 41.

(15) Newns, D. M. *Phys. Rev.* **1969**, *178* (3), 1123.

(16) Hu, P.; King, D. A.; Lee, M. H.; Payne, M. C. *Chem. Phys. Lett.* **1995**, *246* (1−2), 73−78.

(17) Kinoshita, I.; Misu, A.; Munakata, T. *J. Chem. Phys.* **1995**, *102* (7), 2970−2976.

(18) Johnson, P. D.; Hulbert, S. L. *Phys. Rev. B* **1987**, *35* (18), 9427−9436.

(19) Dose, V. *Surf. Sci. Rep.* **1985**, *5*, 337−378.

(20) Kresse, G.; Gil, A.; Sautet, P. *Phys. Rev. B* **2003**, *68* (7), 073401.

(21) Köhler, L.; Kresse, G. *Phys. Rev. B* **2004**, *70* (16), 165405.

(22) Baerends, E. J.; Ros, P. *Int. J. Quantum Chem.* **1978**, *S12*, 169−190.

(23) Fenske, R. F.; DeKock, R. L. *Inorg. Chem.* **1972**, *11* (3), 437−444.

(24) Enemark, J.; Feltham, R. *Coord. Chem. Rev.* **1974**, *13*, 339−406.

(25) Total energy calculations were performed using the DFT-slab approach with a GGA-PBE functional, implemented with the program CASTEP. The Ir{111} surface was modeled by a four-layer slab with top layer relaxed; x and y are coordinates within the surface layer. To mimic the effect a bending of the Ir−N−O group would have on the N−O stretch frequency, the y coordinate of the oxygen atom is fixed at various positions, while all other parameters are allowed to relax.

(26) Lane, I.; King, D.; Arnolds, H. *J. Chem. Phys.* **2007**, *126*, 024707.

(27) Arnolds, H.; Symonds, J. P. R.; Zhang, V. L.; King, D. A. *Rev. Sci. Instrum.* **2003**, *74* (9), 3943−3946.

(28) Symonds, J. P. R.; Arnolds, H.; Zhang, V. L.; Fukutani, K.; King, D. A. *J. Chem. Phys.* **2004**, *120* (15), 7158−7164.

(29) Cornish, J. C. L.; Avery, N. R. *Surf. Sci.* **1990**, *235* (2−3), 209−216.

(30) Davis, J. E.; Karseboom, S. G.; Nolan, P. D.; Mullins, C. B. *J. Chem. Phys.* **1996**, *105* (18), 8362−8375.

(31) Fujitani, T.; Nakamura, I.; Kobayashi, Y.; Takahashi, A.; Haneda, M.; Hamada, H. *J. Phys. Chem. B* **2005**, *109* (37), 17603−17607.

(32) Hamers, R. J.; Houston, P. L.; Merrill, R. P. *J. Chem. Phys.* **1988**, *88* (10), 6548−6555.

(33) Zhang, V. L.; Arnolds, H.; King, D. A. *Surf. Sci.* **2005**, *587* (1−2), 102−109.

(34) Lauterbach, J.; Boyle, R. W.; Schick, M.; Mitchell, W. J.; Meng, B.; Weinberg, W. H. *Surf. Sci.* **1996**, *350* (1−3), 32−44.

(35) Comrie, C. M.; Weinberg, W. H. *J. Chem. Phys.* **1976**, *64* (1), 250−259.

(36) Persson, B. N. J.; Hoffmann, F. M.; Ryberg, R. *Phys. Rev. B* **1986**, *34* (4), 2266−2283.

(37) Witte, G. *J. Chem. Phys.* **2001**, *115* (6), 2757−2767.

(38) We have recorded CO transients for coverages from ca. 0.2 ML up to saturation coverage and find that their temporal shape is independent of coverage.

(39) The −1.5 and 0 ps spectra were recorded 2 h apart, which explains why one common scaling factor for all delay times only describes spectral amplitudes within 20%.

(40) Budde, F.; Heinz, T. F.; Loy, M. M. T.; Misewich, J. A.; Derougemont, F.; Zacharias, H. *Phys. Rev. Lett.* **1991**, *66* (23), 3024−3027.

(41) Culver, J. P.; Li, M.; Sun, Z. J.; Hochstrasser, R. M.; Yodh, A. G. *Chem. Phys.* **1996**, *205* (1−2), 159−166.

(42) Galletto, P.; Unterhalt, H.; Rupprecht, G. *Chem. Phys. Lett.* **2003**, *367* (5−6), 785−790.

(43) Bonn, M.; Denzler, D. N.; Funk, S.; Wolf, M.; Wellershoff, S. S.; Hohlfeld, J. *Phys. Rev. B* **2000**, *61* (2), 1101−1105.

(44) Baldelli, S.; Markovic, N.; Ross, P.; Shen, Y. R.; Somorjai, G. *J. Phys. Chem. B* **1999**, *103* (42), 8920−8925.

(45) Persson, B. N. J.; Gadzuk, J. W. *Surf. Sci.* **1998**, *410* (2−3), L779−L782.

(46) Tully, J. C.; Gomez, M.; Headgordon, M. *J. Vac. Sci. Technol., A* **1993**, *11* (4), 1914−1920.

(47) Lisowski, M.; Loukakos, P. A.; Bovensiepen, U.; Stahler, J.; Gahl, C.; Wolf, M. *Appl. Phys. A* **2004**, *78* (2), 165−176.

(48) Villarrubia, J. S.; Ho, W. *J. Chem. Phys.* **1987**, *87* (1), 750−764.

(49) Sandell, A.; Nilsson, A.; Martensson, N. *Surf. Sci.* **1991**, *241* (1−2), L1−L5.

(50) Shinn, N. D.; Madey, T. E. *J. Chem. Phys.* **1985**, *83* (11), 5928−5944.

(51) Moon, D. W.; Cameron, S.; Zaera, F.; Eberhardt, W.; Carr, R.; Bernasek, S. L.; Gland, J. L.; Dwyer, D. J. *Surf. Sci.* **1987**, *180* (1), L123−L128.

(52) Kaichev, V. V.; Morkel, M.; Unterhalt, H.; Prosvirin, I. P.; Bukhtiyarov, V. I.; Rupprechter, G.; Freund, H. J. *Surf. Sci.* **2004**, *566*, 1024−1029.

(53) Gajdos, M.; Hafner, J.; Eichler, A. *J. Phys.:Condens. Matter* **2006**, *18* (1), 13−40.

(54) Fukutani, K.; Song, M. B.; Murata, Y. *Faraday Discuss.* **1993**, *96* (22), 105−116.

(55) Saalfrank, P.; Boendgen, G.; Finger, K.; Pesce, L. *Chem. Phys.* **2000**, *251* (1−3), 51−69.

(56) Antoniewicz, P. R. *Phys. Rev. B* **1980**, *21* (9), 3811−3815.

(57) Head-Gordon, M.; Tully, J. C. *Phys. Rev. B* **1992**, *46* (3), 1853−1856.

(58) Persson, B. N. J.; Ryberg, R. *Phys. Rev. B* **1985**, *32* (6), 3586−3596.

(59) Anisimov, S. I.; Kapeliov, B.; Perelman, T. L. *Zh. Eksp. Teor. Fiz.* **1974**, *66* (2), 776−781.

(60) Brorson, S. D.; Kazeroonian, A.; Moodera, J. S.; Face, D. W.; Cheng, T. K.; Ippen, E. P.; Dresselhaus, M. S.; Dresselhaus, G. *Phys. Rev. Lett.* **1990**, *64* (18), 2172−2175.

(61) Kittel, C. *Introduction to Solid State Physics,* 7th ed.; John Wiley: New York, 1996.

(62) Baria, J. K.; Jani, A. R. *Physica B* **2003**, *328* (3−4), 317−335.

(63) Allen, P. B.; Pickett, W. E.; Krakauer, H. *Phys. Rev. B* **1987**, *36* (7), 3926−3929.